



Cite this: *Chem. Sci.*, 2025, **16**, 5512

All publication charges for this article have been paid for by the Royal Society of Chemistry

## *In situ* uncovering the catalytic cycle of electrochemical and chemical oxygen reduction mediated by an iron porphyrin†

Xianhao Zhang,‡<sup>ac</sup> Jirui Zhan,‡<sup>a</sup> Haonan Qin,‡<sup>b</sup> Jintao Deng,<sup>a</sup> Junjie Liu,<sup>a</sup> Meixian Li, <sup>a</sup> Rui Cao \*<sup>b</sup> and Yuanhua Shao \*<sup>a</sup>

As one of the critical reactions in biotransformation and energy conversion processes, the oxygen reduction reaction (ORR) catalyzed by iron porphyrins has been widely explored by electrochemical, spectroscopic, and theoretical methods. However, experimental identification of all proposed intermediates of iron porphyrins in one catalytic cycle is rather challenging in the mechanistic studies of the ORR driven by electrochemical or chemical methods. Herein, we report the application of electrochemical mass spectrometry (EC-MS) and chemical reaction mass spectrometry (CR-MS) to *in situ* uncover the catalytic cycle of electrochemical and chemical ORRs mediated by an iron porphyrin molecular catalyst. Five crucial iron–oxygen intermediates detected by both EC-MS and CR-MS help to build the whole catalytic cycle and indicate the details of the  $4e^-/4H^+$  pathway to produce  $H_2O$  in the electrochemical and chemical ORRs. By combining *in situ* MS methods with electrochemical and spectroscopic methods to characterize the intermediates and study the selectivities, this work provides a mechanistic comparison of the electrochemical and chemical ORRs catalyzed by one model iron porphyrin.

Received 7th January 2025  
Accepted 24th February 2025

DOI: 10.1039/d5sc00102a  
[rsc.li/chemical-science](http://rsc.li/chemical-science)

## Introduction

The oxygen ( $O_2$ ) reduction reaction (ORR) is a critical step in biotransformation and energy conversion processes, including biological respiration,<sup>1,2</sup> fuel cells,<sup>3,4</sup> metal–air batteries,<sup>5,6</sup> etc. Inspired by the heme active sites in natural cytochrome c oxidases,<sup>2</sup> iron porphyrins have been widely used and studied as molecular catalysts for the ORR.<sup>7–26</sup> This simplified model reaction helps researchers to better understand the mechanisms and structure–activity relationships of the ORR under controlled conditions with different catalyst ligands, solvents, and proton/electron sources. Depending on electron sources, the ORR catalyzed by molecular complexes can be driven by electrodes or chemical reductants such as ferrocene derivatives.<sup>21,27</sup> Accordingly, most of the previous *in situ* characterization studies in this field investigated the kinetics and mechanisms of the ORR by electrochemical, spectroscopic, and microscopy methods assisted by theoretical calculations.<sup>19,28–46</sup>

Furthermore, the evidence of a series of reactive iron–oxygen intermediates has also been obtained through spectroscopic methods in single-turnover experiments mainly under extremely low temperatures (Table S1 in the ESI†).<sup>47–52</sup> However, the identification of all possible key intermediates proposed in one complete cycle under catalytic conditions is important but inadequate in either the electrochemical or chemical ORR catalyzed by iron porphyrins,<sup>12,18,28–31,33,43,45</sup> which limits comprehensive comparison and understanding of the mechanistic details of the ORR driven by electrochemical and chemical methods. Therefore, developing and applying novel *in situ* characterization methods to detect as many intermediates as possible under electrochemical and chemical conditions is urgently necessary to reveal the mechanism of the ORR catalyzed by molecular complexes including iron porphyrins.

Mass spectrometry (MS) is a powerful analytical technique to characterize analytes with high sensitivity and selectivity, which is widely employed in monitoring chemical/electrochemical reactions and in elucidating their mechanisms by detecting intermediates and products.<sup>53–58</sup> Dual micropipettes pulled from glass theta capillaries are commonly applied as micro-reactors, sampling collectors, and spray emitters in MS analysis.<sup>59–67</sup> Utilizing hybrid ultramicroelectrodes (UMEs) fabricated from dual micropipettes, the *in situ* electrochemical mass spectrometry (EC-MS) developed by Shao and Luo *et al.* has been applied in the mechanistic studies of a series of complicated electrochemical reactions.<sup>68–73</sup> The *in situ* MS method based on dual micropipettes and hybrid UMEs would

<sup>a</sup>Beijing National Laboratory for Molecular Sciences, College of Chemistry and Molecular Engineering, Peking University, Beijing 100871, China. E-mail: yhshao@pku.edu.cn

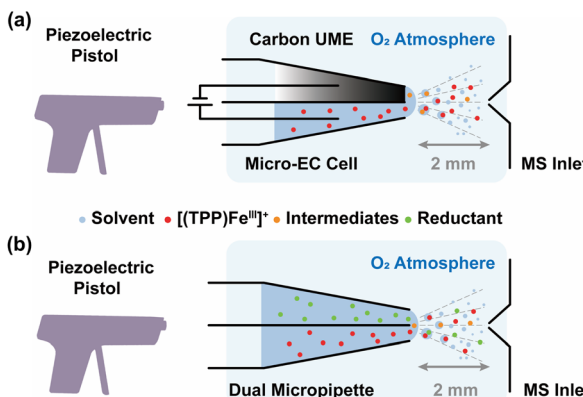
<sup>b</sup>Key Laboratory of Applied Surface and Colloid Chemistry, Ministry of Education, School of Chemistry and Chemical Engineering, Shaanxi Normal University, Xi'an 710119, China. E-mail: ruicao@snnu.edu.cn

<sup>†</sup>Department of Chemistry, China Agricultural University, Beijing 100193, China

† Electronic supplementary information (ESI) available. See DOI: <https://doi.org/10.1039/d5sc00102a>

‡ These authors have contributed equally.





Scheme 1 Schematic illustration of the *in situ* MS setups to study (a) electrochemical and (b) chemical ORRs mediated by  $[(\text{TPP})\text{Fe}^{\text{III}}]^+$ .

be an effective tool to identify intermediates and investigate mechanisms in both chemical and electrochemical ORRs.

Herein, we apply EC-MS based on hybrid UMEs and chemical reaction mass spectrometry (CR-MS) recently developed by our group<sup>74</sup> to *in situ* reveal the mechanism of the ORR mediated by a molecular catalyst 5,10,15,20-meso-tetraphenylporphyrin iron(III) perchlorate ( $[(\text{TPP})\text{Fe}^{\text{III}}]\text{ClO}_4$ ) (Scheme 1). Five key suggested intermediates involved in the electrochemical/chemical ORR were simultaneously detected for the first time by both *in situ* MS methods, providing full experimental evidence and mechanistic details to build the whole catalytic cycle of the ORR mediated by  $[(\text{TPP})\text{Fe}^{\text{III}}]^+$ .<sup>29,31,33</sup> Assisted by electrochemical and spectroscopic methods to determine the selectivity, the same five iron-oxygen intermediates ( $[(\text{TPP})\text{Fe}^{\text{III}}-\text{O}_2\cdot^-]$ ,  $[(\text{TPP})\text{Fe}^{\text{III}}-\text{O}_2\text{H}]^+$ ,  $[(\text{TPP})\text{Fe}^{\text{III}}-\text{O}_2\text{H}_2]^+$ ,  $[(\text{TPP})\text{Fe}^{\text{V}}=\text{O}]^+$ , and  $[(\text{TPP})\text{Fe}^{\text{IV}}-\text{OH}]^+$ ) detected with the exact chemical compositional information by both EC-MS and CR-MS suggest a good agreement of a  $4\text{e}^-/4\text{H}^+$  mechanism in the electrochemical and chemical ORRs catalyzed by  $[(\text{TPP})\text{Fe}^{\text{III}}]^+$ . This work provides a methodology containing two sets of complementary methods to characterize the intermediates and study the mechanisms of electrochemical/chemical redox reactions mediated by molecular catalysts, including the ORR catalyzed by iron porphyrins.

## Results and discussion

### Electrochemical ORR

The electrochemical ORR mediated by  $[(\text{TPP})\text{Fe}^{\text{III}}]^+$  was studied by voltammetry and *in situ* EC-MS. The electrochemical behaviors of  $[(\text{TPP})\text{Fe}^{\text{III}}]\text{ClO}_4$  as an ORR molecular catalyst were first investigated on the carbon hybrid UME in *N,N*-dimethylformamide (DMF) with excess perchloric acid ( $\text{HClO}_4$ ) as the proton source in the absence and presence of  $\text{O}_2$  (Cell 1 in the ESI†). The carbon hybrid UME was fabricated from quartz dual micropipettes according to the reported procedures (Fig. S1†).<sup>73,75</sup> In the cyclic voltammetry (CV) results (Fig. 1), black (1 atm  $\text{N}_2$ ) and red (1 atm  $\text{O}_2$ ) curves show the potential windows of the carbon UME using Cell 1 without  $[(\text{TPP})\text{Fe}^{\text{III}}]^+$

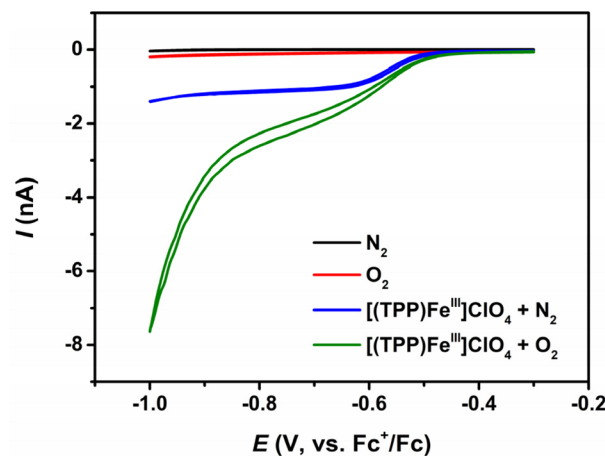


Fig. 1 CV curves of 0.5 mM  $[(\text{TPP})\text{Fe}^{\text{III}}]\text{ClO}_4$  in the absence (blue) and presence (green) of 1 atm  $\text{O}_2$  on a carbon UME in DMF (Cell 1). Black (with  $\text{N}_2$ ) and red (with  $\text{O}_2$ ) curves are the potential windows of the carbon UME using Cell 1 without  $[(\text{TPP})\text{Fe}^{\text{III}}]\text{ClO}_4$ .

$\text{ClO}_4$ . When  $[(\text{TPP})\text{Fe}^{\text{III}}]\text{ClO}_4$  was added under 1 atm  $\text{N}_2$ , a new reversible steady-state curve (blue) emerged, which could be ascribed to the reduction of  $[(\text{TPP})\text{Fe}^{\text{III}}]^+$  to  $[(\text{TPP})\text{Fe}^{\text{II}}]$  (the half-wave potential  $E_{1/2} = -0.55$  V vs.  $\text{Fc}^+/\text{Fc}$ ). When  $[(\text{TPP})\text{Fe}^{\text{III}}]\text{ClO}_4$  was added under 1 atm  $\text{O}_2$ , the CV curve (green) showed much higher currents than in the presence of  $[(\text{TPP})\text{Fe}^{\text{III}}]^+$  and  $\text{N}_2$  (blue), indicating the occurrence of the catalytic ORR. The electrochemical ORR mediated by  $[(\text{TPP})\text{Fe}^{\text{III}}]^+$  on the carbon UME is comparable to those observed on the glassy carbon (GC) electrode in previous reports,<sup>29,41</sup> which proves that the redox state of  $[(\text{TPP})\text{Fe}^{\text{III}}]^+$  can be controlled to catalyze the ORR by applying the potential on the carbon UME under steady-state conditions. Furthermore, the selectivity of the electrochemical ORR mediated by  $[(\text{TPP})\text{Fe}^{\text{III}}]\text{ClO}_4$  was also studied by rotating ring-disk voltammetry (RRDV) under the same conditions (Cell 2 in the ESI†). The results of RRDV prove that the catalytic ORR (GC disk current) occurred and a trace of  $\text{H}_2\text{O}_2$  (Pt ring current) was generated simultaneously when the voltage was less than  $-0.55$  V vs.  $\text{Fc}^+/\text{Fc}$  (Fig. S2†). The average number of electrons  $n_{\text{cat}}$  transferred in the electrochemical ORR equals  $3.88\text{e}^-/\text{O}_2$  from  $-0.6$  V to  $-0.9$  V vs.  $\text{Fc}^+/\text{Fc}$  (Table S2†). The selectivity studies by RRDV confirmed that the  $4\text{e}^-/4\text{H}^+$  pathway is dominant in the electrochemical ORR catalyzed by  $[(\text{TPP})\text{Fe}^{\text{III}}]\text{ClO}_4$ .

Based on the above results by electrochemical characterization of the ORR mediated by  $[(\text{TPP})\text{Fe}^{\text{III}}]\text{ClO}_4$ , *in situ* EC-MS experiments were performed with Cell 3 (in the ESI†) under 1 atm  $\text{O}_2$  using the oxygenated EC-MS setup which combines hybrid UME techniques and relay electrospray ionization MS (Scheme 1a and Fig. S3†).<sup>68,76</sup> When the voltage of carbon UME was off, only  $[(\text{TPP})\text{Fe}^{\text{III}}]^+ (m/z 668)$ ,  $[(\text{TPP})\text{Fe}^{\text{III}}-\text{DMF}]^+ (m/z 741)$ , and background signals were detected (Fig. S4†). When the voltage was on (at  $-0.6$  V to  $-0.9$  V vs.  $\text{Fc}^+/\text{Fc}$ ), five new signals,  $m/z 684$ ,  $m/z 685$ ,  $m/z 700$ ,  $m/z 701$ , and  $m/z 702$ , could be simultaneously detected by MS along with the catalyst signal (Fig. 2 and S5†). The signals of  $m/z 700$ ,  $m/z 701$ , and  $m/z 702$  differing by  $m/z 1$  probably correspond to the intermediate  $[(\text{TPP})\text{Fe}^{\text{III}}-\text{O}_2]^+$  (ionized from  $[(\text{TPP})\text{Fe}^{\text{III}}-\text{O}_2\cdot^-]$ ) by the principle



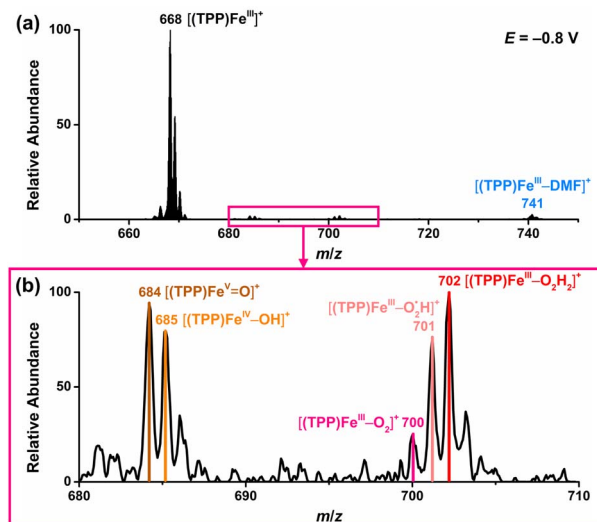


Fig. 2 Mass spectra of the electrochemical ORR catalyzed by  $[(\text{TPP})\text{Fe}^{\text{III}}]^+$  in DMF when the voltage was at  $-0.8\text{ V}$  vs.  $\text{Fc}^+/\text{Fc}$ . (a) Full-scale mass spectra. (b) Zoomed-in mass spectra of iron–oxygen intermediates.

of relay electrospray ionization),<sup>76</sup>  $[(\text{TPP})\text{Fe}^{\text{III}} - \text{O}_2\text{H}]^+$ , and  $[(\text{TPP})\text{Fe}^{\text{III}} - \text{O}_2\text{H}_2]^+$ , respectively. According to the relative abundance, the signal of  $m/z\ 701$  and the signal of  $m/z\ 702$  may contain the isotope peak of  $[(\text{TPP})\text{Fe}^{\text{III}} - \text{O}_2]^+$  and  $[(\text{TPP})\text{Fe}^{\text{III}} - \text{O}_2\text{H}]^+$ , respectively. Likewise, the signal of  $m/z\ 685$  might also correspond to a mixture including the monoisotopic mass peak of  $[(\text{TPP})\text{Fe}^{\text{IV}} - \text{OH}]^+$  and the isotope peak of  $[(\text{TPP})\text{Fe}^{\text{V}} = \text{O}]^+$ . The iron-oxo species could also be of the form  $[(\text{TPP})\text{Fe}^{\text{IV}} = \text{O}]^+$ <sup>77</sup> and we have uniformly represented it in the formal  $[(\text{TPP})\text{Fe}^{\text{V}} = \text{O}]^+$  form in this work. The crucial intermediates  $[(\text{TPP})\text{Fe}^{\text{V}} = \text{O}]^+$  and  $[(\text{TPP})\text{Fe}^{\text{IV}} - \text{OH}]^+$  detected by EC-MS indicate that the electrochemical ORR catalyzed by  $[(\text{TPP})\text{Fe}^{\text{III}}]^+$  involves a  $4\text{e}^-/4\text{H}^+$  pathway to produce  $\text{H}_2\text{O}$  under the described conditions.

### Chemical ORR

For the chemical ORR mediated by  $[(\text{TPP})\text{Fe}^{\text{III}}]^+$ , stopped-flow UV-vis spectroscopy was first used to detect the intermediates and study the selectivity. The experiments were performed by mixing a solution of air-saturated DMF containing  $0.05\text{ mM}$   $[(\text{TPP})\text{Fe}^{\text{III}}]\text{ClO}_4$  and  $5\text{ mM}$   $\text{HClO}_4$  with an equal volume of an air-saturated DMF solution of  $5\text{ mM}$  decamethylferrocene ( $\text{Me}_{10}\text{Fc}$ ) in a stopped-flow instrument.<sup>41</sup> Fig. 3a shows that the signals of iron porphyrin intermediates gradually changed with the increasing concentration of  $\text{Me}_{10}\text{Fc}^+$  ( $715\text{ nm}$ ), suggesting the occurrence of the catalytic ORR. By comparing the results with known spectra of iron porphyrins,<sup>78</sup> the intermediate of  $\text{Fe}^{\text{II}}$  can be identified, while the spectra of other intermediates are overlapped and cannot be distinguished. The selectivity of the chemical ORR catalyzed by  $[(\text{TPP})\text{Fe}^{\text{III}}]\text{ClO}_4$  was indicated by determining the amount of  $\text{Me}_{10}\text{Fc}^+$  produced in the ORR. The results in Fig. 3b suggest that the  $n_{\text{cat}}$  consumed in the chemical ORR equals  $3.90\text{e}^-/\text{O}_2$ , which is close to that in the electrochemical ORR.

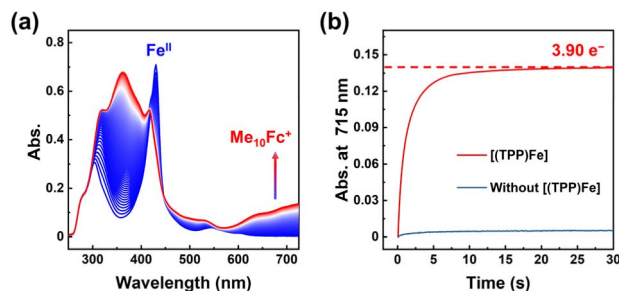


Fig. 3 (a) UV-vis spectra observed during the chemical ORR with  $[(\text{TPP})\text{Fe}^{\text{III}}]\text{ClO}_4$ . (b) Time profiles of the  $\text{Me}_{10}\text{Fc}^+$  formation during the chemical ORR with and without  $[(\text{TPP})\text{Fe}^{\text{III}}]\text{ClO}_4$ .

To further investigate the mechanism of the chemical ORR catalyzed by  $[(\text{TPP})\text{Fe}^{\text{III}}]^+$  in DMF, *in situ* CR-MS experiments were performed with  $10\text{ mM}$   $\text{Me}_{10}\text{Fc}$  and  $1\text{ mM}$   $[(\text{TPP})\text{Fe}^{\text{III}}]\text{ClO}_4$  separately in each barrel of a quartz dual micropipette reactor under  $1\text{ atm}$   $\text{O}_2$  using the same oxygenated MS setup (Scheme 1b and Fig. S3†).  $\text{HClO}_4$  ( $5\text{ mM}$ ) and  $[\text{Bu}_4\text{N}]^+[\text{PF}_6]^-$  ( $10\text{ mM}$ ) were added in both barrels of the dual micropipette. Fig. S6† shows that only  $[(\text{TPP})\text{Fe}^{\text{III}}]^+$  ( $m/z\ 668$ ),  $[(\text{TPP})\text{Fe}^{\text{III}} - \text{DMF}]^+$  ( $m/z\ 741$ ), and background signals were detected when no  $\text{Me}_{10}\text{Fc}$  was added. When the reductant  $\text{Me}_{10}\text{Fc}$  was added, the signals of the five intermediates,  $[(\text{TPP})\text{Fe}^{\text{V}} = \text{O}]^+$  ( $m/z\ 684$ ),  $[(\text{TPP})\text{Fe}^{\text{IV}} - \text{OH}]^+$  ( $m/z\ 685$ ),  $[(\text{TPP})\text{Fe}^{\text{III}} - \text{O}_2]^+$  ( $m/z\ 700$ ),  $[(\text{TPP})\text{Fe}^{\text{III}} - \text{O}_2\text{H}]^+$  ( $m/z\ 701$ ), and  $[(\text{TPP})\text{Fe}^{\text{III}} - \text{O}_2\text{H}_2]^+$  ( $m/z\ 702$ ) were simultaneously detected by MS (Fig. 4). The detected species of iron–oxygen intermediates in the chemical ORR are the same as those in the electrochemical ORR, which proves the same  $4\text{e}^-/4\text{H}^+$  mechanism in the ORR driven by both the electrode and the chemical reductant. Additionally, it should be pointed out that the peaks of  $m/z\ 686$  and  $m/z\ 703$  in both electrochemical and chemical ORRs are attributed to the second strongest isotopic peaks of MS spectra for  $[(\text{TPP})\text{Fe}^{\text{IV}} - \text{OH}]^+$  and  $[(\text{TPP})\text{Fe}^{\text{III}} - \text{O}_2\text{H}_2]^+$ , respectively.

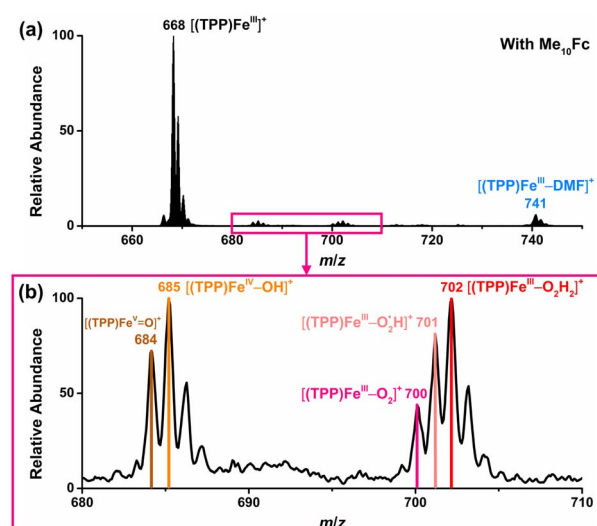
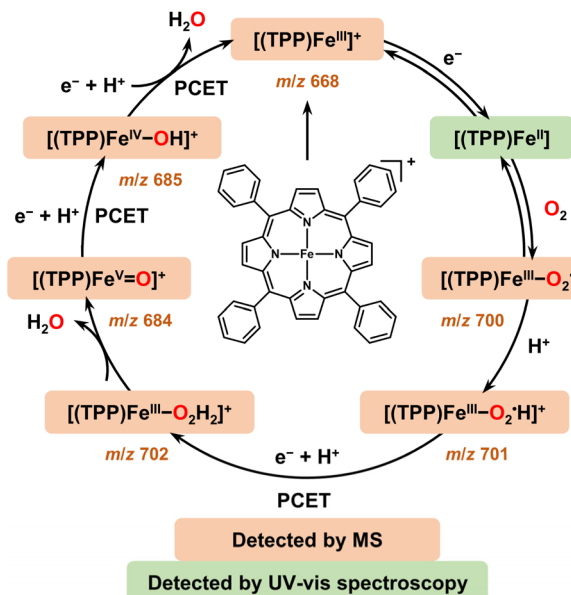


Fig. 4 Mass spectra of the chemical ORR catalyzed by  $[(\text{TPP})\text{Fe}^{\text{III}}]^+$  with  $\text{Me}_{10}\text{Fc}$  as the reductant in DMF. (a) Full-scale mass spectra. (b) Zoomed-in mass spectra of iron–oxygen intermediates.

## Isotope-labeling experiments and ORR mechanism

To further confirm the iron–oxygen intermediates, isotope-labeling electrochemical and chemical ORRs were performed and measured by *in situ* MS, using  $^{18}\text{O}_2$  (97 atom%  $^{18}\text{O}$ ) in place of  $^{16}\text{O}_2$  under the same conditions. As shown in Fig. 5,  $[(\text{TPP})\text{Fe}^{\text{V}}=^{18}\text{O}]^+$  ( $m/z$  686),  $[(\text{TPP})\text{Fe}^{\text{III}}-^{18}\text{O}_2]^+$  ( $m/z$  704), and  $[(\text{TPP})\text{Fe}^{\text{III}}-^{18}\text{O}_2\text{H}_2]^+$  ( $m/z$  706) were all detected by MS in both electrochemical and chemical ORRs, while  $[(\text{TPP})\text{Fe}^{\text{IV}}-^{18}\text{OH}]^+$  ( $m/z$  687) can only be identified in the electrochemical ORR because its signal intensity is much higher than the relative abundance of the second strongest isotopic peak of  $[(\text{TPP})\text{Fe}^{\text{V}}=^{18}\text{O}]^+$ . In addition, possible  $[(\text{TPP})\text{Fe}^{\text{III}}-^{18}\text{O}_2\text{H}]^+$  cannot be identified in the isotopic experiments due to the signal intensity of  $m/z$  705 being close to that of the second strongest isotopic peak of  $[(\text{TPP})\text{Fe}^{\text{III}}-^{18}\text{O}_2]^+$ .

According to the above *in situ* EC-MS/CR-MS, RRDV, and UV-vis spectroscopy results, five iron–oxygen intermediates, including  $[(\text{TPP})\text{Fe}^{\text{III}}-\text{O}_2\cdot^-]$ ,  $[(\text{TPP})\text{Fe}^{\text{III}}-\text{O}_2\cdot\text{H}]^+$ ,  $[(\text{TPP})\text{Fe}^{\text{III}}-\text{O}_2\text{H}_2]^+$ ,  $[(\text{TPP})\text{Fe}^{\text{V}}=\text{O}]^+$ , and  $[(\text{TPP})\text{Fe}^{\text{IV}}-\text{OH}]^+$ , are experimentally confirmed to be produced in both electrochemical and chemical ORRs catalyzed by  $[(\text{TPP})\text{Fe}^{\text{III}}]^+$ . Scheme 2 shows the proposed mechanism of the  $4\text{e}^-/4\text{H}^+$  ORR based on the experimental results in this work and kinetic analysis in previous reports.<sup>31,33,77</sup> Note that we used formal oxidation/reduction states to assign these intermediates. In the catalytic cycle of the ORR with  $[(\text{TPP})\text{Fe}^{\text{III}}]^+$  as the catalyst,  $[(\text{TPP})\text{Fe}^{\text{III}}]^+$  is first reduced by the electrode or  $\text{Me}_{10}\text{Fc}$  to give  $[(\text{TPP})\text{Fe}^{\text{II}}]$ . After that,  $[(\text{TPP})\text{Fe}^{\text{II}}]$  binds an  $\text{O}_2$  molecule to produce the ferric superoxide  $[(\text{TPP})\text{Fe}^{\text{III}}-\text{O}_2\cdot^-]$ , and then  $[(\text{TPP})\text{Fe}^{\text{III}}-\text{O}_2\cdot^-]$  is protonated to form  $[(\text{TPP})\text{Fe}^{\text{III}}-\text{O}_2\cdot\text{H}]^+$ .<sup>31,33</sup> The perhydroxyl complex  $[(\text{TPP})\text{Fe}^{\text{III}}-\text{O}_2\cdot\text{H}]^+$  is next protonated at the distal oxygen along with 1 eq. electron (proton-coupled electron transfer, PCET) to form  $[(\text{TPP})\text{Fe}^{\text{III}}-\text{O}_2\text{H}_2]^+$  and then  $[(\text{TPP})\text{Fe}^{\text{III}}-\text{O}_2\text{H}_2]^+$  releases 1 eq.  $\text{H}_2\text{O}$  to produce  $[(\text{TPP})\text{Fe}^{\text{V}}=\text{O}]^+$ .<sup>12,20</sup> Subsequently,  $[(\text{TPP})\text{Fe}^{\text{V}}=\text{O}]^+$  undergoes successive PCET processes to produce  $[(\text{TPP})\text{Fe}^{\text{IV}}-\text{OH}]^+$  and  $[(\text{TPP})\text{Fe}^{\text{III}}]^+$  along with 1 eq.  $\text{H}_2\text{O}$



Scheme 2 Proposed mechanism of the  $4\text{e}^-/4\text{H}^+$  ORR with  $[(\text{TPP})\text{Fe}^{\text{III}}]^+$  as the catalyst.<sup>12,20,31,33,77</sup>

to finally restart the catalytic cycle of the ORR.<sup>77</sup> Among these intermediates,  $[(\text{TPP})\text{Fe}^{\text{III}}-\text{O}_2\text{H}_2]^+$  is the key to determining the selectivity of the ORR catalyzed by  $[(\text{TPP})\text{Fe}^{\text{III}}]^+$  and its exact configuration has two possible forms ( $[(\text{TPP})\text{Fe}^{\text{III}}-\text{OOH}_2]^+$  and  $[(\text{TPP})\text{Fe}^{\text{III}}-\text{HOOH}]^+$ ).<sup>12</sup> In the  $4\text{e}^-/4\text{H}^+$  pathway, the water could be produced *via* the  $[(\text{TPP})\text{Fe}^{\text{III}}-\text{OOH}_2]^+$  configuration. For the ORR catalyzed by  $[(\text{TPP})\text{Fe}^{\text{III}}]^+$ , the main difference between electrochemical and chemical-driven methods is the resource of electrons, one is from the electrode, and the other is from the reductant. The consistent results of the mechanism and selectivity together confirm the agreement of the ORR driven by these two methods.

## Conclusions

In summary, we have investigated the mechanism of the electrochemical/chemical ORR catalyzed by  $[(\text{TPP})\text{Fe}^{\text{III}}]\text{ClO}_4$  using *in situ* EC-MS/CR-MS assisted by electrochemical characterization and stopped-flow UV-vis spectroscopy. The crucial iron–oxygen intermediates detected by *in situ* MS give detailed experimental evidence to establish the complete catalytic cycle of the ORR with  $[(\text{TPP})\text{Fe}^{\text{III}}]^+$  as a molecular catalyst and indicate a  $4\text{e}^-/4\text{H}^+$  mechanism of this reaction, further supplementing the mechanistic details lacking in previous studies.<sup>29,31,33</sup> This work provides a set of systematical *in situ* analytical methods to study the mechanisms of electrochemical and chemical redox reactions mediated by molecular catalysts. Future work needs to try more kinds of hybrid UMEs and explore the mechanisms of PCET reactions mediated by other molecular catalysts, not limited to the ORR.

## Data availability

All experimental data are available in the manuscript and ESI.†

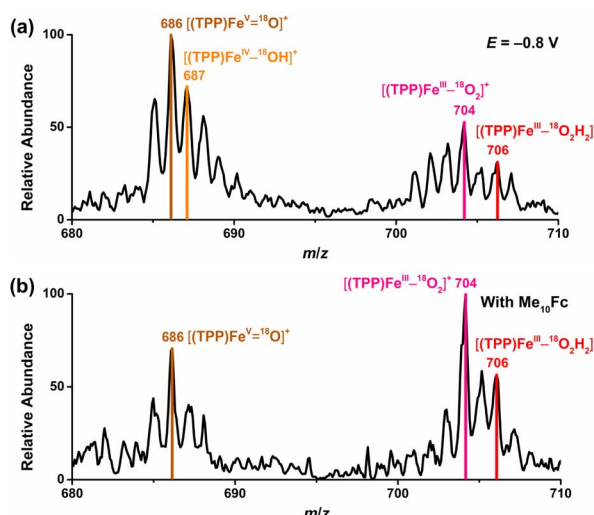


Fig. 5 Mass spectra of  $^{18}\text{O}_2$ -labeling (a) electrochemical and (b) chemical ORRs catalyzed by  $[(\text{TPP})\text{Fe}^{\text{III}}]^+$ .



## Author contributions

Y. Shao and R. Cao conceived and designed the project. X. Zhang and J. Zhan developed the *in situ* mass spectrometry techniques. Y. Shao supervised the experiments of electrochemistry and mass spectrometry. R. Cao supervised the catalyst synthesis and the experiments of UV-vis spectroscopy. X. Zhang and J. Zhan carried out the experiments of electrochemistry and mass spectrometry. H. Qin carried out the experiments of catalyst synthesis and UV-vis spectroscopy. J. Deng assisted in the experiments of electrochemistry and mass spectrometry. All authors contributed to the discussion of the results and the preparation of the manuscript.

## Conflicts of interest

The authors declare no conflict of interest.

## Acknowledgements

This work was supported by the National Natural Science Foundation of China (22034001, 22304003, 22325202, and 22171176), the Beijing National Laboratory for Molecular Sciences (BNLMS-CXXM-202008), and Research Funds of Shaanxi Normal University. We thank Prof. Yan Li and Dr Jian Sheng at Peking University for their help on RRDV experiments.

## References

- 1 G. T. Babcock and M. Wikström, *Nature*, 1992, **356**, 301–309.
- 2 S. Yoshikawa and A. Shimada, *Chem. Rev.*, 2015, **115**, 1936–1989.
- 3 Y. Li, M.-Y. Chen, B.-A. Lu and J.-N. Zhang, *J. Electrochem.*, 2023, **29**, 2215002.
- 4 S. Li, L. Shi, Y. Guo, J. Wang, D. Liu and S. Zhao, *Chem. Sci.*, 2024, **15**, 11188–11228.
- 5 F. Cheng and J. Chen, *Chem. Soc. Rev.*, 2012, **41**, 2172–2192.
- 6 Y. Su, Z. Zhao, J. Huang, E. Wang and Z. Peng, *J. Phys. Chem. C*, 2022, **126**, 1243–1255.
- 7 M. L. Rigsby, D. J. Wasylenko, M. L. Pegis and J. M. Mayer, *J. Am. Chem. Soc.*, 2015, **137**, 4296–4299.
- 8 Y. Xuan, X. Huang and B. Su, *J. Phys. Chem. C*, 2015, **119**, 11685–11693.
- 9 X. Huang, Y. Xuan, L. Xie and B. Su, *ChemElectroChem*, 2016, **3**, 1781–1786.
- 10 S. Bhunia, A. Rana, P. Roy, D. J. Martin, M. L. Pegis, B. Roy and A. Dey, *J. Am. Chem. Soc.*, 2018, **140**, 9444–9457.
- 11 A. Ghatak, S. Bhakta, S. Bhunia and A. Dey, *Chem. Sci.*, 2019, **10**, 9692–9698.
- 12 A. C. Brezny, S. I. Johnson, S. Raugei and J. M. Mayer, *J. Am. Chem. Soc.*, 2020, **142**, 4108–4113.
- 13 A. Singha, A. Mondal, A. Nayek, S. G. Dey and A. Dey, *J. Am. Chem. Soc.*, 2020, **142**, 21810–21828.
- 14 A. C. Brezny, H. S. Nedzbala and J. M. Mayer, *Chem. Commun.*, 2021, **57**, 1202–1205.
- 15 B. D. Groff and J. M. Mayer, *ACS Catal.*, 2022, **12**, 11692–11696.
- 16 S. Bhunia, A. Ghatak, A. Rana and A. Dey, *J. Am. Chem. Soc.*, 2023, **145**, 3812–3825.
- 17 D. Nishiori, J. P. Menzel, N. Armada, E. A. Reyes Cruz, B. L. Nannenga, V. S. Batista and G. F. Moore, *J. Am. Chem. Soc.*, 2024, **146**, 11622–11633.
- 18 A. K. Surendran, A. Y. Pereverzev and J. Roithová, *J. Am. Chem. Soc.*, 2024, **146**, 15619–15626.
- 19 S. Chatterjee, K. Sengupta, B. Mondal, S. Dey and A. Dey, *Acc. Chem. Res.*, 2017, **50**, 1744–1753.
- 20 W. Zhang, W. Lai and R. Cao, *Chem. Rev.*, 2017, **117**, 3717–3797.
- 21 M. L. Pegis, C. F. Wise, D. J. Martin and J. M. Mayer, *Chem. Rev.*, 2018, **118**, 2340–2391.
- 22 H. Lei, X. Li, J. Meng, H. Zheng, W. Zhang and R. Cao, *ACS Catal.*, 2019, **9**, 4320–4344.
- 23 C. W. Machan, *ACS Catal.*, 2020, **10**, 2640–2655.
- 24 Y. Li, N. Wang, H. Lei, X. Li, H. Zheng, H. Wang, W. Zhang and R. Cao, *Coord. Chem. Rev.*, 2021, **442**, 213996.
- 25 S. Bhunia, A. Ghatak and A. Dey, *Chem. Rev.*, 2022, **122**, 12370–12426.
- 26 X. Li, H. Lei, L. Xie, N. Wang, W. Zhang and R. Cao, *Acc. Chem. Res.*, 2022, **55**, 878–892.
- 27 A. W. Nichols, E. N. Cook, Y. J. Gan, P. R. Miedaner, J. M. Dressel, D. A. Dickie, H. S. Shafaat and C. W. Machan, *J. Am. Chem. Soc.*, 2021, **143**, 13065–13073.
- 28 K. Sengupta, S. Chatterjee, S. Samanta and A. Dey, *Proc. Natl. Acad. Sci. U. S. A.*, 2013, **110**, 8431–8436.
- 29 D. J. Wasylenko, C. Rodríguez, M. L. Pegis and J. M. Mayer, *J. Am. Chem. Soc.*, 2014, **136**, 12544–12547.
- 30 C. Costentin, H. Dridi and J.-M. Savéant, *J. Am. Chem. Soc.*, 2015, **137**, 13535–13544.
- 31 M. L. Pegis, B. A. McKeown, N. Kumar, K. Lang, D. J. Wasylenko, X. P. Zhang, S. Raugei and J. M. Mayer, *ACS Cent. Sci.*, 2016, **2**, 850–856.
- 32 C. Costentin and J.-M. Savéant, *J. Am. Chem. Soc.*, 2018, **140**, 16669–16675.
- 33 M. L. Pegis, D. J. Martin, C. F. Wise, A. C. Brezny, S. I. Johnson, L. E. Johnson, N. Kumar, S. Raugei and J. M. Mayer, *J. Am. Chem. Soc.*, 2019, **141**, 8315–8326.
- 34 Y. Liu, G. Zhou, Z. Zhang, H. Lei, Z. Yao, J. Li, J. Lin and R. Cao, *Chem. Sci.*, 2020, **11**, 87–96.
- 35 A. Facchini, T. Kosmala, A. Gennaro and C. Durante, *ChemElectroChem*, 2020, **7**, 1431–1437.
- 36 J. Meng, H. Qin, H. Lei, X. Li, J. Fan, W. Zhang, U.-P. Apfel and R. Cao, *Angew. Chem., Int. Ed.*, 2023, **62**, e202312255.
- 37 J. Han, H. Tan, K. Guo, H. Lv, X. Peng, W. Zhang, H. Lin, U.-P. Apfel and R. Cao, *Angew. Chem., Int. Ed.*, 2024, **63**, e202409793.
- 38 T. Liu, H. Qin, Y. Xu, X. Peng, W. Zhang and R. Cao, *ACS Catal.*, 2024, **14**, 6644–6649.
- 39 A. Facchini, D. Forrer, M. Zerbetto, F. Cazzadore, A. Vittadini and C. Durante, *ACS Catal.*, 2024, **14**, 14373–14386.
- 40 A. Santra, A. Das, S. Kaur, P. Jain, P. P. Ingole and S. Paria, *Chem. Sci.*, 2024, **15**, 4095–4105.
- 41 H. Qin, J. Kong, X. Peng, Z. Wang, X. Li, H. Lei, W. Zhang and R. Cao, *ChemSusChem*, 2025, **18**, e202401739.
- 42 C. Costentin, *Chem. Rev.*, 2008, **108**, 2145–2179.

43 J.-M. Savéant, *Chem. Rev.*, 2008, **108**, 2348–2378.

44 C. Costentin, M. Robert and J.-M. Savéant, *Chem. Rev.*, 2010, **110**, PR1–PR40.

45 K. Sengupta, S. Chatterjee and A. Dey, *ACS Catal.*, 2016, **6**, 6838–6852.

46 C. Costentin and J.-M. Savéant, *Nat. Rev. Chem.*, 2017, **1**, 0087.

47 J.-G. Liu, Y. Shimizu, T. Ohta and Y. Naruta, *J. Am. Chem. Soc.*, 2010, **132**, 3672–3673.

48 Z. Halime, H. Kotani, Y. Li, S. Fukuzumi and K. D. Karlin, *Proc. Natl. Acad. Sci. U. S. A.*, 2011, **108**, 13990–13994.

49 M. T. Kieber-Emmons, M. F. Qayyum, Y. Li, Z. Halime, K. O. Hodgson, B. Hedman, K. D. Karlin and E. I. Solomon, *Angew. Chem., Int. Ed.*, 2012, **51**, 168–172.

50 H. Kim, P. J. Rogler, S. K. Sharma, A. W. Schaefer, E. I. Solomon and K. D. Karlin, *J. Am. Chem. Soc.*, 2020, **142**, 3104–3116.

51 S. Samanta, S. Sengupta, S. Biswas, S. Ghosh, S. Barman and A. Dey, *J. Am. Chem. Soc.*, 2023, **145**, 26477–26486.

52 E. E. Chufán, S. C. Puiu and K. D. Karlin, *Acc. Chem. Res.*, 2007, **40**, 563–572.

53 A. Ray, T. Bristow, C. Whitmore and J. Moseley, *Mass Spectrom. Rev.*, 2018, **37**, 565–579.

54 D. Freitas, X. Chen, H. Cheng, A. Davis, B. Fallon and X. Yan, *ChemPlusChem*, 2021, **86**, 434–445.

55 W. Li, J. Sun, Y. Gao, Y. Zhang, J. Ouyang and N. Na, *TrAC, Trends Anal. Chem.*, 2021, **135**, 116180.

56 J. Sun, Y. Yin, W. Li, O. Jin and N. Na, *Mass Spectrom. Rev.*, 2022, **41**, 70–99.

57 X. Zhang, J. Zhan, Z. Yu, J. Deng, M. Li and Y. Shao, *Chin. J. Chem.*, 2023, **41**, 214–224.

58 K. Chen, Q. Wan, S. Wei, W. Nie, S. Zhou and S. Chen, *Chem.-Eur. J.*, 2024, **30**, e202402215.

59 L. P. Mark, M. C. Gill, M. Mahut and P. J. Derrick, *Eur. J. Mass Spectrom.*, 2012, **18**, 439–446.

60 D. N. Mortensen and E. R. Williams, *Anal. Chem.*, 2014, **86**, 9315–9321.

61 D. N. Mortensen and E. R. Williams, *J. Am. Chem. Soc.*, 2016, **138**, 3453–3460.

62 R. M. Bain, S. Sathyamoorthi and R. N. Zare, *Angew. Chem., Int. Ed.*, 2017, **56**, 15083–15087.

63 E. T. Jansson, Y.-H. Lai, J. G. Santiago and R. N. Zare, *J. Am. Chem. Soc.*, 2017, **139**, 6851–6854.

64 A. Saha-Shah, J. A. Karty and L. A. Baker, *Analyst*, 2017, **142**, 1512–1518.

65 N. Sahota, D. I. AbuSalim, M. L. Wang, C. J. Brown, Z. Zhang, T. J. El-Baba, S. P. Cook and D. E. Clemmer, *Chem. Sci.*, 2019, **10**, 4822–4827.

66 Y. Li, L. Meng, G. Wang, X. Zhou, Z. Ouyang and Z. Nie, *Anal. Chem.*, 2020, **92**, 12049–12054.

67 L. A. Baker and G. S. Jagdale, *Curr. Opin. Electrochem.*, 2019, **13**, 140–146.

68 R. Qiu, X. Zhang, H. Luo and Y. Shao, *Chem. Sci.*, 2016, **7**, 6684–6688.

69 W. Guo, H. Ding, C. Gu, Y. Liu, X. Jiang, B. Su and Y. Shao, *J. Am. Chem. Soc.*, 2018, **140**, 15904–15915.

70 C. Gu, X. Nie, J. Jiang, Z. Chen, Y. Dong, X. Zhang, J. Liu, Z. Yu, Z. Zhu, J. Liu, X. Liu and Y. Shao, *J. Am. Chem. Soc.*, 2019, **141**, 13212–13221.

71 M. Li, P. He, Z. Yu, S. Zhang, C. Gu, X. Nie, Y. Gu, X. Zhang, Z. Zhu and Y. Shao, *Anal. Chem.*, 2021, **93**, 1515–1522.

72 Z. Yu, Y. Shao, L. Ma, C. Liu, C. Gu, J. Liu, P. He, M. Li, Z. Nie, Z. Peng and Y. Shao, *Adv. Mater.*, 2022, **34**, 2106618.

73 X. Zhang, Q.-F. Chen, J. Deng, X. Xu, J. Zhan, H.-Y. Du, Z. Yu, M. Li, M.-T. Zhang and Y. Shao, *J. Am. Chem. Soc.*, 2022, **144**, 17748–17752.

74 Q.-F. Chen, X. Zhang, J. Shi, J. Zhan, F. Xie, H.-T. Zhang, J. Deng, J. Liu, M. Li, Y. Shao and M.-T. Zhang, *CCS Chem.*, 2025, **7**, 893–904.

75 Y. Takahashi, A. I. Shevchuk, P. Novak, Y. Zhang, N. Ebejer, J. V. Macpherson, P. R. Unwin, A. J. Pollard, D. Roy, C. A. Clifford, H. Shiku, T. Matsue, D. Klenerman and Y. E. Korchev, *Angew. Chem., Int. Ed.*, 2011, **50**, 9638–9642.

76 A. Li, A. Hollerbach, Q. Luo and R. G. Cooks, *Angew. Chem., Int. Ed.*, 2015, **54**, 6893–6895.

77 X. Huang and J. T. Groves, *Chem. Rev.*, 2018, **118**, 2491–2553.

78 P. Mondal, I. Ishigami, S.-R. Yeh and G. B. Wijeratne, *Angew. Chem., Int. Ed.*, 2022, **61**, e202211521.

